NANO LETTERS

2005
Vol. 5, No. 11
2268−2273

Structural Transformations of Carbon Nanotubes under Hydrostatic Pressure

Paul Tangney,*,† Rodrigo B. Capaz,‡,§,|| Catalin D. Spataru,‡,§ Marvin L. Cohen,‡,§ and Steven G. Louie†,‡,§

The Molecular Foundry, Lawrence Berkeley National Laboratory, Berkeley, California 94720, Department of Physics, University of California, Berkeley, CA 94720, Materials Sciences Division, Lawrence Berkeley National Laboratory, Berkeley, CA 94720, and Instituto de Física, Universidade Federal do Rio de Janeiro, Caixa Postal 68528, Rio de Janeiro, RJ 21941-972, Brazil

Received August 18, 2005; Revised Manuscript Received September 26, 2005

ABSTRACT

We used simulations with a classical force field to study the transformation under hydrostatic pressure of isolated single-walled nanotubes (SWNT) from a circular to a collapsed cross section. Small-diameter SWNTs deform continuously under pressure, whereas larger-diameter SWNTs display hysteresis and undergo a first-order-like transformation. The different behavior is due to the changing proportions in the total energy of the wall-curvature energy and the van der Waals attraction between opposite walls of the tube.

The study of pressure effects on the structure of single-wall carbon nanotubes (SWNTs) is a topic of much recent interest.[1] High-pressure experiments on bundles suggest the occurrence of symmetry-breaking transitions at critical pressures ranging from 1.5 GPa to 2.1 GPa for laser-grown tubes ($d \approx 12-14$Å)[2−4] and at 6.6 GPa for HiPCo tubes ($d \approx 8$Å).[5] In a previous work,[6] we have shown that this behavior is related to an intrinsic property of *isolated* SWNTs, namely, the instability of the circular cross section at the critical pressure with respect to squashing deformations. Similar results have been obtained by other authors.[7−9] There have been recent proposals to use this property of isolated SWNTs for building nanoscale pressure sensors.[10]

In this work, we investigate the deformation in more detail. A more complex picture emerges: isolated SWNTs show three qualitatively different behaviors under pressure depending on the tube diameter, d. For "large" diameters, SWNTs collapse at a critical pressure, P_d, with a discontinuous change in volume, in contrast to predictions from elasticity theory that suggest a continuous (although abrupt) deformation beyond a critical pressure.[8,11,12] We identify the van der Waals interaction between the opposite walls of the SWNT as the driving force for this behavior. For "small" diameters, the transformation is continuous, from a circle to an oval cross section (with the deformation onset occurring at a pressure, P_c) and with a gradual change to "racetrack" and "peanut" shapes as the pressure increases. Finally, for "intermediate" diameters, the continuous transformation at P_c is followed by a discontinuous one at P_d.

We perform zero-temperature structural minimizations and classical molecular dynamics (MD) simulations at 300 K for SWNTs under hydrostatic pressure. The carbon−carbon bonding (elastic energy) in the SWNTs is modeled by the extended Tersoff−Brenner potential.[13] Pairwise Lennard−Jones potentials model the nonbonding van der Waals term.[14] The technical aspects of our constant pressure MD simulations are similar to those of Martonak et al.:[15] The nanotubes are immersed in a pressure-transmitting medium of particles interacting via a repulsive A/r^{12} potential. Pressure and viscosity are monitored in a 314-Å^3 subunit cell that contains only medium particles, and the pressure is changed by varying the strength of the interaction between the medium particles. The strength of the interaction between medium particles and the carbon atoms is kept fixed at $A = 130$ eV Å^{12} for all of our simulations.

MD simulations are performed under periodic boundary conditions with unit cells of 30-Å width in each of the directions perpendicular to the tube axis. In the axial direction, the length depends on the size of the unit cell for the nanotube in question, but for zigzag tubes we use eight unit cells and therefore a length of approximately 34 Å. The number of medium particles in the box varies because of nanotubes of different radii occupying different proportions of the total volume, but it was typically around 3 000. The mass of the medium particles is set at 5 amu.

* Corresponding author. E-mail: pttangney@lbl.gov; fax: 510-643-9478.
† The Molecular Foundry, Lawrence Berkeley National Laboratory.
‡ Department of Physics, University of California, Berkeley.
§ Materials Sciences Division, Lawrence Berkeley National Laboratory.
|| Universidade Federal do Rio de Janeiro.

10.1021/nl051637p CCC: $30.25
Published on Web 10/15/2005

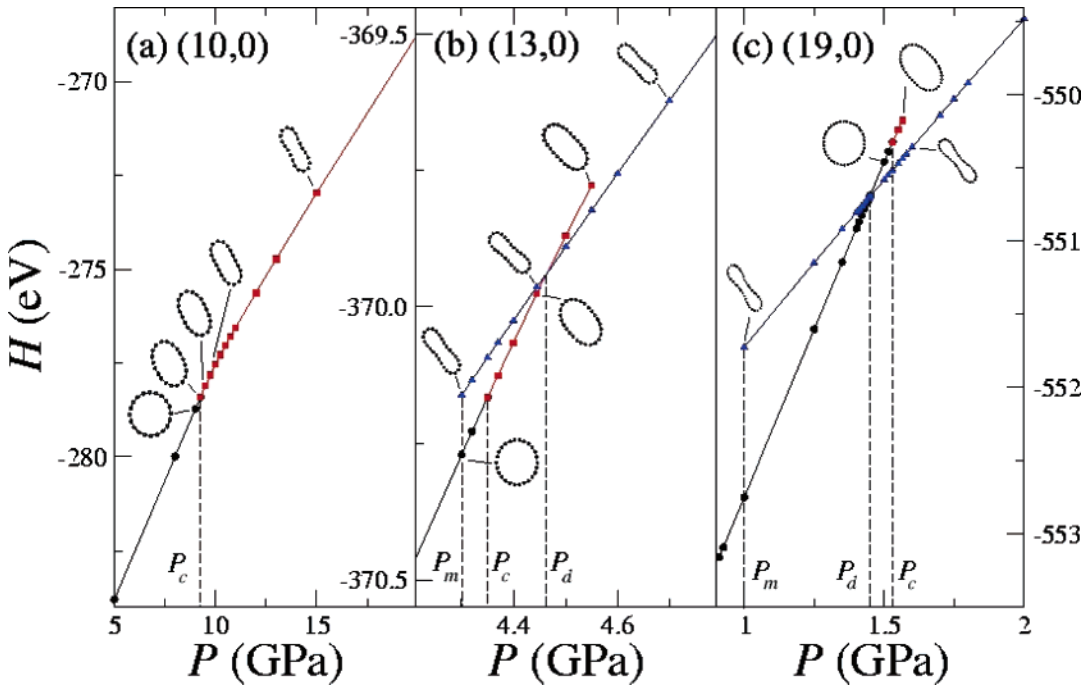

Figure 1. Enthalpy vs pressure for the (a) (10,0), (b) (13,0), and (c) (19,0) SWNTs. Black dots indicate a circular cross section, red squares indicate the oval and collapsed (for the (10,0) SWNT) structures, and the blue triangles indicate the collapsed (peanut-like) structures. Only points corresponding to structures that are local minima of the enthalpy are plotted in all cases. The straight lines connecting consecutive points are intended as a guide to the eye. Critical pressures, P_m, P_d and P_c, are indicated by dashed lines. Cross-sectional shapes are shown at a variety of pressures in all three cases.

To perform zero-temperature structural minimizations of the enthalpy ($H = U + PV$), one needs to define the volume of the nanotube. There is no rigorous or unique way to geometrically define the volume of a molecule; however, this task is greatly facilitated in the case of nanotubes because of their axial geometry. In particular, zigzag tubes have polygonal cross sections that allow their cross-sectional areas to be written as functions of the atomic positions, $\{R_I\}$, even if changes in bond lengths and angles are permitted. Once the volume is thus defined, the contribution to the force on each ion, I, arising from the PV term of the enthalpy is simply $-P(\partial V/\partial R_I)$. Therefore, for simplicity, we will focus our study on zigzag tubes. However, our main conclusions should be easily generalized for all SWNTs because their mechanical properties do not vary strongly with chirality. We also note that a sensible definition of a molecular volume should take into account a small correction in volume due to the electronic cloud surrounding the atoms.[6] This correction is neglected in our $T = 0$ K minimizations but is naturally included in the MD simulations. At a given pressure, local minima of the enthalpy for both the circular and collapsed nanotube configurations are sought by performing a combination of conjugate gradient and steepest descent enthalpy minimizations. These minimizations are started from nearby structural configurations such as the corresponding minimum enthalpy configurations at lower or higher pressures or those obtained from finite temperature molecular dynamics simulations.

We use the nudged-elastic-band (NEB) method[16] to find the minimum-enthalpy transformation path between circular and collapsed geometries for a variety of zigzag SWNTs and at a variety of pressures. The end points of the NEB minimization at a given pressure are the SWNTs of circular and collapsed cross sections for which the enthalpy is a local minimum (or a local maximum in the case of circular SWNTs at high pressures). These end points have been connected by an "elastic band" containing 200 beads. We note that the transformation path that we calculate is the transformation path for *uniform* deformation of a nanotube, and the enthalpy barriers calculated are the enthalpy barriers per unit cell for such a uniform deformation. The enthalpy barrier for uniform deformation is proportional to the length of the nanotube and is therefore prohibitively large. Therefore, we do not expect the true minimum-enthalpy deformation path to be a uniform deformation but rather a deformation that nucleates locally and propagates along the tube axis in a highly nonuniform manner. We therefore attach meaning only to the relative enthalpies of the local minima along the transformation path and to the existence, or nonexistence, of enthalpy barriers.

Figure 1a−c shows the enthalpy as a function of pressure for the (10,0), (13,0), and (19,0) SWNTs, respectively. As we shall see, these are prototype examples of small-, intermediate-, and large-diameter tubes. The points plotted are only those corresponding to structures that are local *minima* of the enthalpy. For the (10,0) tube, the curve has only one branch, thus indicating the existence of a single stable geometry for each pressure. At $P = P_c$, a subtle kink in the plot indicates the onset of a continuous transformation between a circular (black dots) and an oval (red squares) cross section, as indicated in the figure. As the pressure increases, the cross-sectional area decreases and the oval

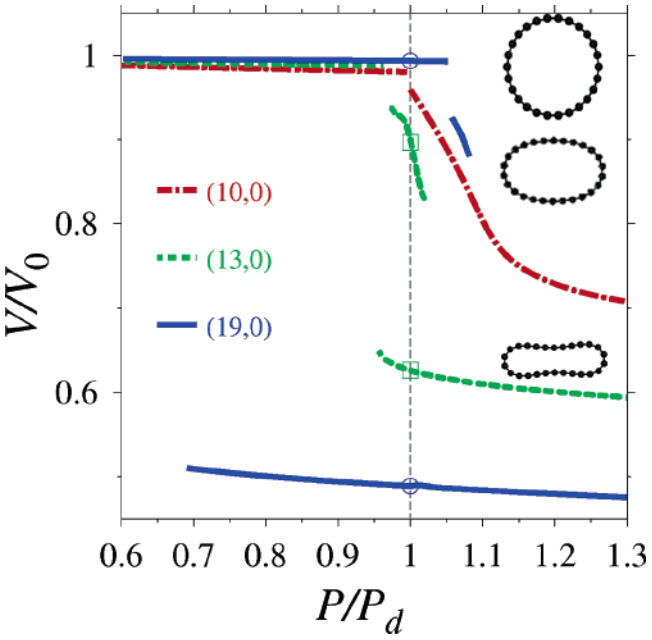

Figure 2. Volume (scaled by the volume at zero pressure V_0) as a function of pressure (scaled by P_d, or P_c for the (10,0) tube) for the (10,0), (13,0), and (19,0) nanotubes from zero-temperature enthalpy minimizations. The lines connect configurations corresponding to local or global enthalpy minima and terminate at pressures at which a given structure (circle, oval, or peanut) either becomes unstable or, in the case of the oval structure at pressures close to P_c, cannot be stabilized for numerical reasons. The dashed vertical line indicates where a first-order-like structural transformation is predicted to occur between structures on different branches of the $P-V$ plot (indicated by matching symbols) for the (13,0) and (19,0) nanotubes.

deforms continuously into a racetrack and then into a peanut shape. For the (13,0) and (19,0) SWNTs, the situation is qualitatively different. For a certain range of pressures, one can obtain two metastable structures: a circle or oval and a collapsed (racetrack or peanut) structure. One can therefore define three critical pressures, P_m, P_d, and P_c as indicated in the figure. Pressure P_m marks the onset of metastability of the peanut shape: at pressures slightly lower than P_m a large number of enthalpy minimizations were performed, starting from different initial configurations, but the collapsed structure always reverted to a circular shape. The critical pressure, P_d, is the pressure for which the enthalpy of the two configurations are equal (i.e., for $P > P_d$ the peanut is the most stable structure) and at which a discontinuous transformation between circle (or oval) and peanut may occur. Finally, P_c is the pressure at which the circular shape becomes unstable with respect to an oval shape, just as in the small-diameter SWNTs.

These three different behaviors can also be seen from a PV diagram, shown in Figure 2. The lines indicate the scaled pressures and volumes of stable or metastable structures. Different lines for a given SWNT correspond to the different metastable structures: circle, oval, and peanut. Matching open symbols indicate points on different branches of the PV plot that have the same enthalpy. At $P = P_d$, a discontinuous (first-order-like) transformation is predicted to occur for the (13,0) and (19,0) tubes between these points.

If one neglects the tiny pressure range near P_c where energy differences were too small to be resolved in our simulations, the PV curve for the (10,0) SWNT appears to consist of a single branch, and therefore, as discussed above, the transformation from circle to oval to peanut is continuous. The (13,0) and (19,0) SWNTs, however, both have features of first-order transformations: a discontinuous variation in volume and a hysteresis loop. For the (13,0) SWNT, the discontinuous change in volume occurs after a continuous transformation from a circular to an ovular cross section has already taken place. For the (19,0) SWNT, there is a discontinuous transformation directly from a circular cross section to a peanut cross section and the oval cross section, which is metastable over a small pressure range at zero temperature, is unlikely ever to be observed in an experiment.

In Figure 3a, the enthalpy difference, ΔH, (with respect to the circular configuration) along the minimum enthalpy transformation paths between the circular and peanut-shaped configurations of the (13,0) SWNT are plotted. At 4.3 GPa, the circular configuration (at the far right-hand side of the plot) is clearly the configuration of minimum enthalpy, whereas the collapsed structure (on the far left) appears to be a shallow local minimum. As pressure increases, the local minimum corresponding to the peanut structure becomes more pronounced and lowers in enthalpy relative to the enthalpy of the circle. Furthermore, the circular cross section gradually changes from a local (and global) minimum to a local maximum as a new local minimum appears with a volume that is intermediate between that of the circular and fully collapsed SWNT. As illustrated for the case of $P = 4.445$ GPa $\approx P_d$, this minimum corresponds to a SWNT with an oval-shaped cross section. As the pressure increases further, the peanut-shaped SWNT becomes the global minimum (at P_d) and gradually the barrier between the oval and the peanut is lowered until, at high pressures, only the peanut shape is stable. In Figure 3b, the different contributions to ΔH along the minimum enthalpy transformation path at $P = 4.445$ GPa $\approx P_d$ are plotted. The elastic (Tersoff–Brenner) and PV terms make the largest contributions to ΔH, but at P_d they almost cancel one another so that the small excess of elastic energy is comparable in magnitude to the van der Waals energy.

The different behavior of large- and intermediate-diameter SWNTs can now be understood by recognizing the role of the van der Waals interaction in stabilizing the collapsed geometry. Nanotubes have "sticky walls" because of the van der Waals interaction and, for large-diameter tubes, this contribution to the energy can be large enough to stabilize the peanut structure at pressures for which the contribution to ΔH of the PV term of the deformed structure ($P\Delta V$) is still smaller than the contribution of the elastic energy (ΔU_{el}). The contribution of the van der Waals energy (ΔU_{vdw}) to ΔH increases approximately linearly with the circumference of the nanotube and therefore ΔU_{vdw} per atom varies slowly with diameter. The proportion of the total number of bonds that need to bend significantly to deform a nanotube into a peanut or oval shape decreases as the tube circumference

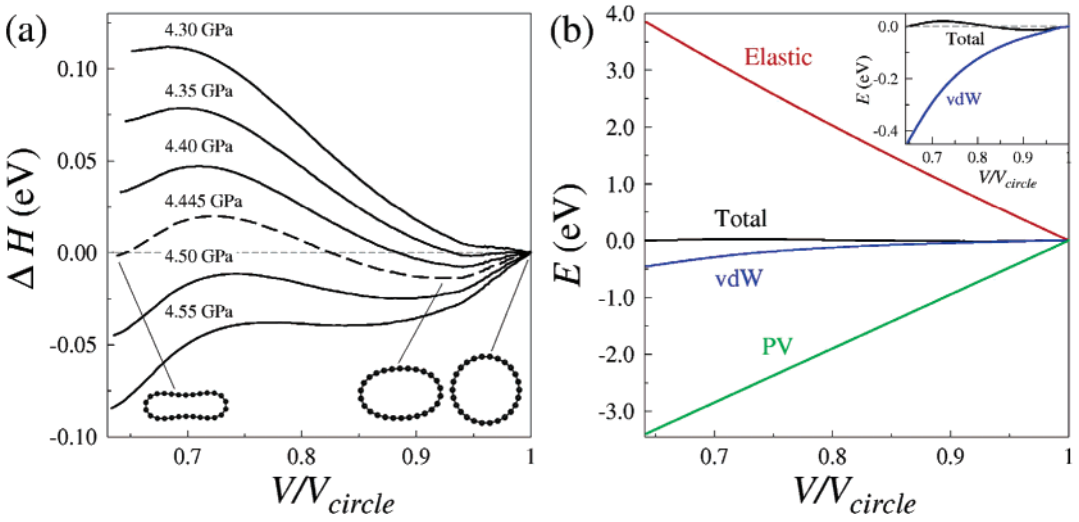

Figure 3. (a) Enthalpy difference per unit cell ($\Delta H = H - H_{circle}$) as a function of scaled volume V/V_{circle} of the (13,0) SWNT at a variety of pressures along the minimum enthalpy transformation path between circular and collapsed configurations. At each pressure, H_{circle} and V_{circle} are the enthalpy and the volume of the (stable or unstable) equilibrium circular configuration for that pressure. (b) Different contributions to ΔH for the (13,0) SWNT along the lowest enthalpy path between the circular and collapsed configurations at $P = 4.445$ GPa, which is very close to P_d. The inset highlights the total ΔH and the contribution from the van der Waals energy.

increases so that ΔU_{el} per atom is significantly larger for small nanotubes. This means that, as one decreases the diameter, the ratio of ΔU_{vdw} to ΔU_{el} (and to $P\Delta V$ close to $P = P_d$) decreases. As one decreases the diameter, therefore, the range of pressures for which the van der Waals energy is sufficient to overcome the excess elastic energy decreases and P_m gets closer and closer to P_d. For the (10,0) tube, the range of metastability of the peanut structure below P_d is too small for us to resolve in our simulations.

To further illustrate the crucial role played by the van der Waals energy in producing the diameter-dependent behavior of nanotubes under pressure, we look at the behavior of the (19,0) tube in the absence of van der Waals interactions. We perform a series of enthalpy minimizations of the (19,0) tube under pressure using a potential energy that only includes the Tersoff−Brenner covalent bonding energy. The results are presented in Figure 4. It is found that the result of omitting the Lennard−Jones potential is that the (19,0) nanotube shows a qualitative behavior that is identical to small-diameter tubes such as the (10,0). At a certain critical pressure, P_c , the nanotube begins a continuous deformation from the circular shape to an oval shape to a fully collapsed peanut shape. As expected, given that the diameter of the (19,0) tube is large compared to the range of the van der Waals potential, the value of P_c does not change significantly when this interaction is omitted. The peanut structure is no longer found to be metastable, and therefore the hysteresis and the existence of a first-order-like transformation disappear. These results are now qualitatively very similar to those of previous works.[5,8,9] The inset of Figure 4b shows that there is a dramatic change in the shape and volume of the nanotube within a small pressure range close to P_c and that there is a tiny enthalpy difference between the circular and deformed nanotubes over this pressure range. The large decrease in PV during the initial stages of deformation appears to be almost entirely canceled by the increase in the elastic energy.

As discussed above, the magnitude of the change in elastic energy per atom due to bond-bending, ΔU_{el}, decreases with increasing diameter. Until the peanut shape is reached, the change in PV due to deformation is approximately equal to $P\Delta V$ because of the large change in volume and the very small pressure range in which the deformation occurs. Therefore, the magnitude of $\Delta(PV)$ per atom is roughly proportional to the ratio of the change in the cross-sectional area of the nanotube to its (approximately constant) perimeter, and therefore it increases with diameter.[8] This explains why, in Figure 2, the pressure range of stability of the oval shape, when scaled by P_d , is seen to decrease with increasing diameter. For larger diameters, the PV term dominates the elastic energy more rapidly with changing (P/P_d) than for smaller tubes.

Figure 5 shows the diameter dependence of the critical deformation pressures: they all decrease with increasing diameter, in agreement with previous results.[6−9] Continuum elasticity theory predicts that P_c should decrease as $1/d^3$ in the limit of large d.[11,12] From our data between $d = 7$ Å and $d = 15$ Å, we find a power law $1/d^{2.9}$, in excellent agreement with that prediction. However, P_m and P_d should go exactly to zero at finite diameters: for SWNTs with diameters $d >$ 23 Å, the collapsed structure is locally metastable at zero pressure, and it becomes the ground state for $d >$ 34 Å.[17−19] In other words, P_m and P_d should decrease with diameter, and they should go exactly to zero near $d = 23$ Å and $d =$ 34 Å, respectively.

The molecular dynamics simulations show that the above description is robust under the introduction of finite temperatures and provide extra insight into the different configurations of carbon nanotubes under pressure. In simulations of larger-radius tubes, both circular and deformed cross sections can be observed near P_d. This is illustrated for the (16,0) tube in movies 1 and 2 of the Supporting Information. These movies show a (16,0) tube at $P \approx P_d$ and $T = 300$ K.

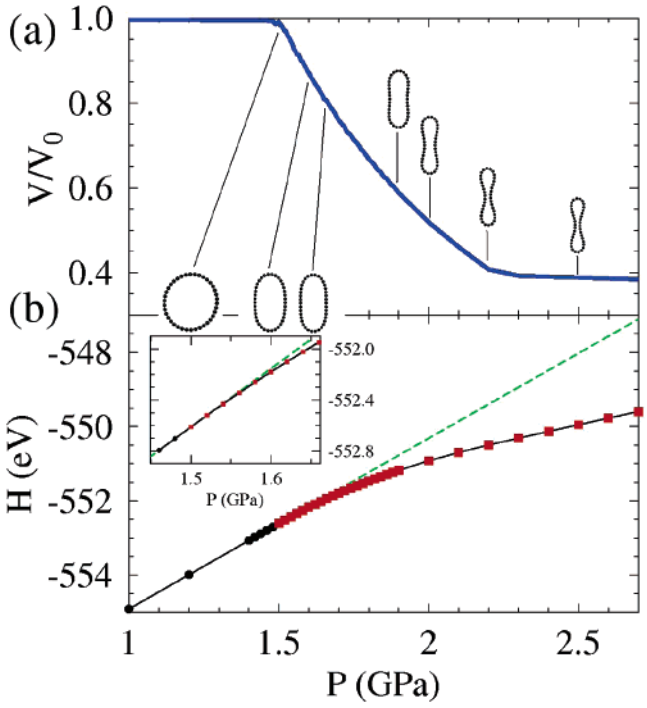

Figure 4. Results of enthalpy minimizations as a function of pressure for the (19,0) nanotube in which the Lennard−Jones potential, U_{vdw}, (which incorporates the van der Waals interaction energy) has been omitted from the potential, U, so that only the Tersoff−Brenner potential describing the elastic energy, U_{el}, remains. (a) Volume (scaled by the volume at zero pressure V_0) as a function of pressure. (b) Enthalpy, $H = U_{el} + PV$, as a function of pressure. Black dots indicate a circular cross section and red squares indicate a deformed cross section. The dashed green line indicates the enthalpy of the nanotube with a circular cross section as a function of pressure. The inset is a plot of H versus P close to the pressure $P_c \approx 1.5$ GPa at which the nanotube starts to deform. The shapes of the nanotube at pressures of 1.5, 1.6, 1.65, 1.8, 2.0, 2.2, and 2.5 GPa are illustrated.

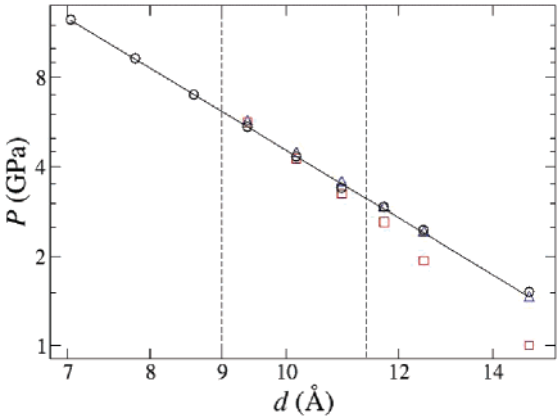

Figure 5. Critical pressures P_m (squares), P_d (triangles), and P_c (circles) as a function of nanotube diameter from zero-temperature enthalpy minimizations.

The two movies illustrate the coexistence of the two phases near the critical pressure. Movie 3 shows a (10,0) SWNT for $P > P_m$, illustrating an oval cross section. Notice that, when symmetry is broken from a circle to an oval, a multiplicity of ground states appears, each corresponding to a different orientation of the oval. The dynamics of the tube at room temperature seems to be dominated by transitions between these ground states.

In summary, using a combination of zero-temperature enthalpy minimization and finite temperature molecular dynamics simulations we have elucidated the nature and mechanism of the transformation of SWNTs from circular to deformed cross sections under hydrostatic pressure. The existence of first-order-like and second-order-like transformations depending on diameter is yet another manifestation of the complexity of nanotubes. It would be interesting to experimentally determine mechanical (e.g., compressibility) and thermal (e.g., heat capacity) response functions of single nanotubes to search for signatures of these different types of structural transformations. The existence of metastable structures and hysteresis loops for large-diameter tubes may complicate their use as nanoscale pressure sensors[10] because their structural properties, and therefore their electrical properties, will not be uniquely defined by the pressure.

Acknowledgment. This work was partially supported by National Science Foundation grant no. DMR04-39768 and by the Director, Office of Science, Office of Basic Energy Sciences, Division of Materials Sciences and Engineering, U.S. Department of Energy under contract no. DE-AC03-76SF00098. R.B.C. acknowledges financial support from the John Simon Guggenheim Memorial Foundation and Brazilian funding agencies CNPq, CAPES, FAPERJ, Instituto de Nanociências, FUJB-UFRJ, and PRONEX-MCT. Computational resources were provided by NPACI and NERSC.

Supporting Information Available: Three movies of our molecular dynamics are available. Movies 1 and 2 are from a simulation of the (16,0) SWNT at P close to P_d. Movie 3 is from a simulation of the (10,0) SWNT at $P > P_c$. This material is available free of charge via the Internet at http://pubs.acs.org.

References

(1) Venkateswaran, U. D. *Phys. Status Solidi B* **2004**, *241*, 3345.
(2) Venkateswaran, U. D.; Rao, A. M.; Richter, E.; Menon, M.; Rinzler, A.; Smalley, R. E.; Eklund, P. C. *Phys. Rev. B* **1999**, *59*, 10928.
(3) Peters, M. J.; McNeil, L. E.; Lu, J. P.; Kahn, D. *Phys. Rev. B* **2000**, *61*, 5939.
(4) Sandler, J.; Shaffer, M. S. P.; Windle, A. H.; Halsall, M. P.; Montes-Morán, M. A.; Cooper, C. A.; Young, R. J. *Phys. Rev. B* **2003**, *67*, 035417.
(5) Elliott, J. A.; Sandler, J. K. W.; Young, R. J.; Windle, A. H.; Shaffer, M. S. P. *Phys. Rev. Lett.* **2004**, *92*, 095501.
(6) Capaz, R. B.; Spataru, C. D.; Tangney, P.; Cohen, M. L.; Louie, S. G. *Phys. Status Solidi B* **2004**, *241*, 3352.
(7) Li, C.; Chou, T.-W. *Phys. Rev. B* **2004**, *69*, 073401.
(8) Zang, J.; Treibergs, A.; Han, Y.; Liu, F. *Phys. Rev. Lett.* **2004**, *92*, 105501.
(9) Sun, D. Y.; Shu, D. J.; Ji, M.; Liu, F.; Wang, M.; Gong, X. G. *Phys. Rev. B* **2004**, *70*, 165417.
(10) Wu., J.; Zang, J.; Larade, B.; Guo, H.; Gong, X. G.; Liu, F. *Phys. Rev. B* **2004**, *69*, 153406.
(11) Carrier, G. F. *J. Math. Phys.* **1947**, *26*, 94.
(12) Chaskalovic, J. *Z. Angew. Math. Phys.* **1995**, *46*, 149.
(13) Brenner, D. W.; Shenderova, O. A.; Harrison, J. A.; Stuart, S. J.; Ni, B.; Sinnott, S. B. *J. Phys.: Condens. Matter* **2002**, *14*, 783.
(14) Ryckaert, J.-P.; Bellemans, A. *Chem. Phys. Lett.* **1975**, *30*, 123.
(15) Martonak, R.; Molteni, C.; Parrinello, M. *Phys. Rev. Lett.* **2000**, *84*, 682.
(16) (a) Mills, G.; Jónsson, H. *Phys. Rev. Lett.* **1994**, *72*, 1124. (b) Henkelman, G.; Jónsson, H. *J. Chem. Phys.* **2000**, *113*, 9978.

(17) Chopra, N. G.; Benedict, L. X.; Crespi, V. H.; Cohen, M. L.; Louie, S. G.; Zettl, A. *Nature (London)* **1995**, *377*, 135.
(18) Benedict, L. X.; Chopra, N. G.; Cohen, M. L.; Zettl, A.; Louie, S. G.; Crespi, V. H. *Chem. Phys. Lett.* **1998**, *286*, 490.
(19) Zhang, P.; Crespi, V. H. *Phys. Rev. Lett.* **1999**, *83*, 1791.

NL051637P